EG UK Theory and Practice of Computer Graphics (2006)
M. McDerby, L. Lever (Editors)

Computing Static Electricity on Human Hair

G. Sobottka A. Weber

Institut für Informatik II, Universität Bonn, Germany

Abstract

We present a framework to study electrical charge phenomena on human hair. We propose a fiber based hair model which bases on the special theory of Cosserat Rods to overcome the well known difficulties one has to deal with when simple particle systems are used. We show how such models can efficiently be employed in conjunction with the fast multipole method to account for Coulomb far-field interactions. Furthermore, we extend our model such that we can account for environmental conditions.

Categories and Subject Descriptors (according to ACM CCS): I.3.6 [Computer Graphics]: Graphics data structures and data types

1. Introduction

Human hair modeling is an active area of research in computer graphics [CK05, SVW05, WGL04, HMT01]. Many of the hair models that have been introduced to the computer graphics community primarily aim at speed rather than accuracy. Using the naturally occurring hierarchy of single hair fibers and hair strands the physical simulation of hair has focussed on the level of hair strands [BKCN03, BCN03]. Only on the geometrical level the strands are then subdivided into single fibers for visualization.

However, for more accurate hair modeling a true hierarchical physical simulation is necessary connecting the level of a hair strands with the finer level of hair fibers also on the physical level and not only the geometrical level.

A physical simulation on the level of single hair fibers is especially important if special physical effects influencing the overall appearance of the hair geometry have to be included. Up to now this is a rather neglected area. Recently, some physical models have been introduced that capture the effects of water and styling products [WGL04]—with a rather limited accuracy. Other very prominent physical effects like that of static electricity on human hair have not been included in any model so far.

In an extreme form the effect is well known from an appealing experiment in physics lesson: A person puts both hands on a Van de Graaf generator. A belt made of plastic or rubber is turned by a motor and builds up a “static charge” by scratching on a wire which is attached to a metal shell. This effect is well known as triboelectricity. The negative charge flows directly from the surface of the metal shell to the surface of the test person. If the hair is clean and dry and the fibers do not stick together due to lipids or moisture on their surface they should start to lift because each fiber has a repelling negative potential. The fibers follow the streamlines of the electric field and take the typical shockheaded hair style.

Also in non-extreme cases the effects of static electricity might visible contribute to the overall appearance of human hair. Even normal combing or brushing causes static electricity in human hair changing the overall hair volume and smoothness in subtle but visible ways. As there are different effects from combing or brushing which cannot be separated empirically from each other highly accurate models are necessary that are capable to predict the effects of static electricity among others.

Our contributions. We introduce a fiber based hair model which can be seen as the first step towards a high accuracy model for hair modeling tasks in general. We employ a static Cosserat model to model single hair fibers and demonstrate how this approach can be combined with a multipole expansion of point charges to capture the effects of static electricity on human hair.

As multipole expansions are little used in computer graphics we will discuss them in Sec. 2.

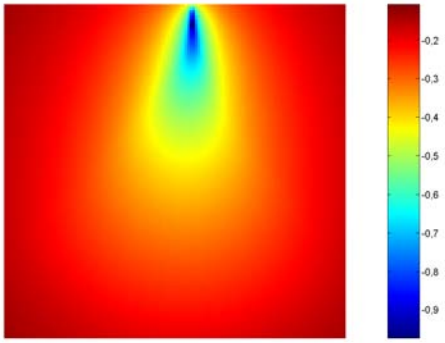

Figure 1: *Potential field of a hair strand computed from discrete point charges on a* $128 \times 128 \times 128$ *grid (cf. results section).*

In Sect. 3 we discuss an equilibrium state rod model based on the special theory of COSSERAT rods that is suitable as a fiber based hair model. Results of coupling the previously introduced fiber based hair model with a computation of electrostatic forces are given in Sect. 4.

2. General Setup for Computing Electrostatic Forces

Electrostatic problems are governed by Coulomb's law. Let the objects of investigation be simple point charges distributed in space. The Coulomb force acting between two point charges located at $\mathbf{x}_1$ and $\mathbf{x}_2$ is given by $\mathbf{f}^C = c_0 \cdot (q_1 \cdot q_2 / |\mathbf{x}_2 - \mathbf{x}_1|^3 \cdot (\mathbf{x}_2 - \mathbf{x}_1))$[†]. In case of many particles the Coulomb interaction follows directly from the principle of superposition which is valid for electrostatic fields:

$$\mathbf{f}^C = c_0 \cdot \sum_{j=1, i \neq j}^{n} \left[q_i \cdot q_j \cdot \frac{\mathbf{x}_i - \mathbf{x}_j}{|\mathbf{x}_i - \mathbf{x}_j|^3} \right]. \tag{1}$$

The main problem of computing electrostatics between a given set of point charges is that the Coulomb mutual interactions of all particles have to be taken into account even if they are far apart from each other. Thus, the complexity is $\mathcal{O}(n^2)$. This is known as the *N-body problem*. Models that account for physical influences due to sources that are far away are normally referred to as *far field* models.

Problems involving many bodies are well known in the computer graphics community as they frequently occur in the realm of collision detection. But these problems should not be confused with the classic N-body problem because the bodies do not interact over a wide range. Collisions and their subsequent responses are a local phenomenon. Thus, strategies to accelerate the computation of pairwise Coulomb interactions cannot rely on spatial or object subdivision techniques alone like in the collision detection problem. Such techniques only allow us to limit the sphere of action and focus on the local interactions. However, simply truncating far-field interactions above a predetermined distance can lead to unphysical behavior as was shown by [DYP93]. What we need is a technique to approximate far-field interactions because intuitively the impact of two adjacent bodies on a third body which is far away should be very similar. The missing link to accomplish this is known in the physics community as *multipole expansion*.

[†] c_0 depends on the choice of units and is equal to 1 for the cgs system.

2.1. The Multipole Expansion

To understand the concept of the multipole expansion of the electrostatic potential consider a point charge q at position $\mathbf{x}_0 \in \mathbb{R}^3$. The potential in the vicinity of the particle is given by $\Phi(\mathbf{x}) = 1/\tilde{r}$, where $\tilde{r} = |\mathbf{x} - \mathbf{x}_0|$ is the distance from the particle. The multipole expansion is a series expansion that expresses the potential $\Phi(\mathbf{x})$ in terms of its distance r from the origin. The adoption of spherical coordinates, $\mathbf{x} = (r, \theta, \varphi)$ and $\mathbf{x}_0 = (\hat{r}, \hat{\theta}, \hat{\varphi})$, leads to an expression in terms of Legendre polynomials:

$$\Phi = 1/\tilde{r} = \sum_{n=0}^{\infty} \hat{r}^n / r^{n+1} P_n(\cos\gamma), \tag{2}$$

where γ is the angle between $\mathbf{x}_0$ and $\mathbf{x}$. This, in turn, can be expressed by a class of functions known as spherical harmonics. These constitute a set of orthogonal solutions to the underlying Laplace equation $\nabla^2 \Phi = 0$ if we consider the problem in spherical coordinates.

We now examine k charges of strength q_i located at the positions $\hat{\mathbf{x}} = (\hat{r}_i, \hat{\theta}_i, \hat{\varphi}_i)$ within a sphere of radius R. The potential for any point $\mathbf{x} = (r, \theta, \varphi)$ outside the sphere is then given by

$$\Phi(\mathbf{x}) = \sum_{n=0}^{\infty} \sum_{m=-n}^{n} \frac{M_n^m}{r^{n+1}} \cdot Y_n^m(\theta, \varphi), \tag{3}$$

where

$$M_n^m = \sum_{i=1}^{k} q_i \cdot \hat{r}_i^n \cdot Y_n^{-m}(\hat{\theta}_i, \hat{\varphi}_i), \tag{4}$$

is the moment of the expansion and accounts for the charge distribution. $Y_n^m(\theta, \varphi)$ are spherical harmonic polynomials of degree n and defined as

$$Y_n^m(\theta, \varphi) = \sqrt{\frac{(n - |m|)!}{(n + |m|)!}} P_n^{|m|}(\cos\theta) e^{im\varphi}, \tag{5}$$

where $P_n^m(x)$ are the associated Legendre polynomials.

The above equations are only valid if the particles are well separated. Further, it is important to note that since these approximations do not converge at close ranges one must

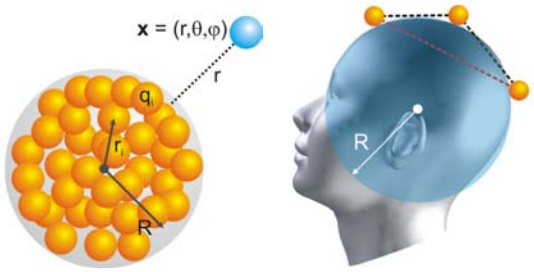

Figure 2: *Left: The outer multipole expansion expresses the potential outside a sphere of radius R due to all particles inside the sphere. Right: Boundary conditions; Interference of particles on opposite sides of the head.*

further explicitly compute near field interactions. If the distance $r >> R$ of a particle is large compared to the radius of the surrounding sphere for which the multipole expansion is to be computed then we approximate the Coulomb interaction with all the particles inside the sphere by evaluating a finite number p of terms in the expansion. Thus, the forces acting at each particle consist of a fraction due to the far field (*ff*) and one due to the near field interactions (*nf*): $\mathbf{f}_\Sigma = \mathbf{f}_{\text{nf}} + \mathbf{f}_{\text{ff}} + \mathbf{f}_{\text{ext}}$, where ext are external forces due to gravity or collision response etc.

The corresponding electrostatic field is given by the gradient of the potential

$$\mathbf{E} = -\nabla\Phi(\mathbf{x}) = -\partial\Phi/\partial x_i. \tag{6}$$

From the electrostatic field we obtain the forces acting on each particle as $\mathbf{F} = q \cdot \mathbf{E}$. An example of a potential field of a hair strand computed with our approach can be seen in Fig. 1.

2.2. Charged Tracer Particles

The multipole expansions have been derived for point charges and it is possible to do the same for other primitives like cylinders or tori. But this is cumbersome and normally not compatible with standard multipole codes. To approximate the charged surface of a thin generalized cylinder with a given length we introduce the concept of *tracer particles*. Therein, each hair fiber is equipped with a set of (negative) point charges. We then compute a multipole expansions of the potential to approximate the far-field interaction of each particle. From this we can deduce the Coulomb force acting on the particles as the gradient of the potential.

It is not clear how the particle density ρ_P can be chosen efficiently. The forces due to Coulomb interactions can be split into a tangential part and a normal part. The tangential part causes the tracer particles to shift along the fiber until a equilibrium is reached. In reality this effect takes place at the speed of light. After redistributing the tracer particles it would be necessary to recompute the the Coulomb interactions until the system of particle converges against a stable equilibrium. However, this modus operandi can become very expensive if the number of particles is large. In practice, we simply choose a constant density for the tracer particles. This density does not necessarily correspond to the node density of the fibers so it is independent of the underlying discretization. The tracer particles are fixed in space and do not move as the corresponding fiber deforms. Thus, it is necessary to map them back to the corresponding positions after each deformation step. For this, we introduce a bijective mapping based on the arc length parameter. Their cartesian coordinates can then be computed by linear interpolation from the coordinates of the nodes to the left and to the right of a particle.

2.3. Multipole Codes

A number of approaches have been proposed by the physics community to tackle the N-body problem. These approaches employ standard space or object partitioning techniques like octrees or bounding volume hierarchies to subdivide the computational domain. The tree like algorithm of Barnes and Hut [BH86] originates from the field of astrophysics and performs at costs of $\mathcal{O}(n \log n)$. The *Fast Multipole Method (FMM)* of Greengard and Rokhlin [GR87] is one of the most successful as it is based on analysis of the pairwise interactions of point charges and allows for a priori error bounds. The computational costs are reduced to $\mathcal{O}(n)$ by introducing the concept of local expansions. The main difference between the FMM and the algorithm of [BH86] is that the former operates with potentials whereas the latter directly computes forces.

2.3.1. The Fast Multipole Method

We decided to base our electrostatic computations on the FMM. First an octree is built on the cloud of tracer particles distributed over the fibers with a given density ρ_P. At the leaves of the tree the multipole expansion is computed directly from all particles within a cell, i.e., from their positions and strengths. The computation of the potential performs in two passes, one upward pass to accumulate the multipole expansions of the cells and one downward pass to compute the potential for each particle inside a cell due to all particles outside the cell. Near field influences are computed concurrently since they only depend on the nearest neighbors which are located in adjacent octree cells.

The total number of operations to be performed is $189(N/s)p^4 + 2np^2 + 27ns$, where s is the average number of particles per leaf node and p is number of terms in the multipole expansion. In order to achieve a desired precision of ε the number of terms that must be evaluated is $p = \log_{\sqrt{3}} 1/\varepsilon$. The translation and conversion of multipole expansions can be justified by foundamental theorems of the

theory of spherical harmonics. We refer the interested reader to the original work of Greengard and Rokhlin [GR87].

2.4. Particle-Surface Interactions

The scalp surface—or the object's surface in general—normally contributes to the overall deformation since it carries its own charge. Moreover, taking into account the repelling forces between the scalp and the hair fibers acts as a form of collision handling as it prevents the fibers from moving into the object. To allow a fast charge computation we calculate for the head surface $\mathcal{S}$ an implicit linear approximation, a distance field Φ_S which is a scalar mapping $\Phi_S : \mathbb{R}^3 \to \mathbb{R}$ such that

$$\Phi_S(\mathbf{x}) := \min_{\mathbf{q}\in\mathcal{S}} \{|\mathbf{x}-\mathbf{q}|\}, \forall \mathbf{q} \in \mathbb{R}^3. \tag{7}$$

Strictly speaking, Coulomb's law applies only to charged particles without extension, but we still use it here for the force computations between the particles and the scalp. Hence, particles in the vicinity of the scalp experience a repelling force which decreases with $1/r^2$. The force is given as

$$\mathbf{f}^S(\mathbf{x}) = \frac{|q_i| \cdot |Q_S|}{r_x^2} \cdot \frac{\nabla\Phi_S(\mathbf{x})}{|\nabla\Phi_S(\mathbf{x})|}, \tag{8}$$

where $\nabla\Phi_S(\mathbf{x})$ is the gradient of the implicit function at $\mathbf{x}$ and r_x the smallest distance of $\mathbf{x}$ to $\mathcal{S}$. Q_S is the surface charge such that $q_i \cdot Q_S > 0$. The implicit approximation of the surface is computed using the method of characteristics. For each triangle of the underlying mesh the Voronoi regions of the face, the edges as well as its vertices are computed. The Voronoi region of a face forms a prism whereas that of a convex edge forms a wedge like area. The Voronoi region of the vertices forms a cone if the vertex is convex. We then compute the distances of each grid point inside a Voronoi region to the respective feature. The distances are stored on a rectilinear grid. The signs are chosen according to the direction of the normal. For a given point $\mathbf{x}$ the distance to the surface can then be calculated in terms of a tri-linear interpolation over the cell's corners in which the point of interest lies. The total costs for the Coulomb force approximation are, thus linear in the number of particles.

In order to prevent singular forces we assume that the initial hair configuration is collision free in the sense that **a)** the tracer particles are well separated (see above) and **b)** none of the tracer particles lies inside the object. If for some reason **b)** is not met the distance has a negative sign. Since the resulting force decreases quadratically with the distance it is possibly to small to push the particle outside the object. In principle, these pathological cases can be detected by a simple sign check of d. We then use a linear or even slower decreasing force.

2.5. Boundary Conditions

Boundary conditions normally need a special handling since the line of action between two particles may theoretically intersect with the boundary. In our case the boundary is constituted by the surface of the human head model. It is normally not possible to incorporate such boundaries into standard multipole codes while maintaining the $\mathcal{O}(n)$ scheme because the multipole expansions are usually computed on a per cell basis. In principle, those interactions could be computed directly and subtracted from the eligible particle's overall charges. However, we assume that the error is very small as it only affects particles that are close to the surface (cf. Fig. 2). Therefore, the bending moment induced in the vicinty of the root of a hair is small. Since the force decreases quadratically the effect on pairs of particles with large distance is negligible.

3. Special Theory of Cosserat Rods

The modeling of long thin structures with torsional stiffness has gained increased attention in the realm of computer graphics. Catheters, cables in microsurgery simulations, and hairs are normally not open for approaches like particle systems. It is difficult to measure local deformations like twist with mass-spring systems or to map material properties to them. Another important aspect is that the temporal evolution of mass-spring approximated materials with high internal viscosity leads to the well known stiff-equation problems. In the realm of hair modeling the research tends to the development of more accurate models. So called rod theories which describe the deformation of long thin solid structures subject to external loads have been developed by KIRCHHOFF [Kir59] and later by the Brothers COSSERAT. The *local director* approach allows one to accurately model local deformations like shear, bending, and twist. Further, material properties can directly be incorporated in terms of so called constitutive relations. Following Antman [Ant95] the equations describing the equilibrium state of a rod can be derived as follows.

3.1. General Setup

Given a smooth space curve $\mathbf{r}(s) : s \subset \mathbb{R} \longrightarrow \mathbb{R}^3$ which describes the center line of a filament in its reference state with s being the arc length parameter. We equip this space curve with a pair of orthonormal directors $\mathbf{d}_1(s)$ and $\mathbf{d}_2(s)$ such that they span the cross section plane at s. This cross section is normal to the curve at s and therefore we obtain a third direction by $\mathbf{d}_3 := \mathbf{d}_1 \times \mathbf{d}_2$. The directors $\mathbf{d}_i$ form a right-handed orthonormal basis for $\mathbb{R}^3$. Furthermore, we assume the existence of vector-valued functions $\mathbf{u}$ and $\mathbf{v}$ such that $\mathbf{d}_k' = \mathbf{u} \times \mathbf{d}_k$ and $\mathbf{r}' = \mathbf{v} \cdot \mathbf{d}_k$, where $(\cdot)'$ denotes the derivative w.r.t. the arc length parameter. The former is normally referred to as kinematic relation. The components of this function are given by $\mathbf{u} = u_k \mathbf{d}_k$ and $\mathbf{r}' = v_k \mathbf{d}_k$. The components

of $\mathbf{u} := (u_1, u_2, u_3)$ and $\mathbf{v} := (v_1, v_2, v_3)$ have physical meanings as they are the strain variables describing the motion of a material cross section through space. The first two components of $\mathbf{u}$ indicate the flexure about $\mathbf{d}_1$ and $\mathbf{d}_2$ and u_3 measures the torsion, i.e. the rotation about the normal of the cross section whereas the components of $\mathbf{v}$ describe the shear and the expansion, respectively. Thus, the centerline $\mathcal{C}$ of the fiber is determined by $\mathbf{r}(s)$, $\mathbf{d}_1(s)$, and $\mathbf{d}_2(s)$, except for a rigid motion, i.e., rotation and translation.

Two degenerate cases can occur in our filament: 1) if we allow the curve to expand arbitrarily it can take local zero length, i.e., $|\mathbf{r}'| = 0$. This can be prevented if we ensure that the expansion always is $v_3 > 0$, thus $\mathbf{r}' \cdot \mathbf{d}_3 > 0$. 2) If we further allow the filament to undergo shear deformation the cross section plane is no longer orthogonal to the centerline. In the extreme case it is tangent to the curve. This can also be prevented by the condition $v_3 > 0$.

To derive the balance laws consider a rod element of length $ds = s^+ - s^-$, with $0 < s^- < s^+ < l$. Then the rod element $(s^+, l]$ exerts a resultant contact force $\mathbf{n}^+(s^+)$ and contact torque $\mathbf{r}(s^+) \times \mathbf{n}^+(s^+) + \mathbf{m}^+(s^+)$ about the origin on the section $[s^-, s^+]$, where $\mathbf{m}^+(s^+)$ is the resultant contact couple. $\mathbf{n}^+(\cdot)$ and $\mathbf{m}^+(\cdot)$ depend only on the separating section between the rod elements $[0, s^-)$ and $(s^+, l]$. The contact force and torque about the origin from the left rod element exerted on $[s^-, s^+]$ are denoted by $-\mathbf{n}^-(s^-)$ and $-\mathbf{r}(s^-) \times \mathbf{n}^-(s^-) - \mathbf{m}^-(s^-)$. Other forces and moments acting on $[s^-, s^+]$ are conveniently expressed in the integral form $\int_a^b \mathbf{f}(s)\mathrm{ds}$ and $\int_a^b [\mathbf{r}(s) \times \mathbf{f}(s) + \mathbf{l}(s)]\mathrm{ds}$, where $\mathbf{f}(s)$ and $\mathbf{l}(s)$ are the body force and couple per unit reference length. From this we obtain the equilibrium equations as

$$\mathbf{n}' + \mathbf{f} = \mathbf{0} \tag{9}$$

$$\mathbf{m}' + \mathbf{r}' \times \mathbf{n} + \mathbf{g} = \mathbf{0}. \tag{10}$$

Since the rod is clamped at one end ($s = 0$) and can freely move at the other we have the following boundary conditions: $\mathbf{x}(0) = \mathbf{x}_0$, $\mathbf{d}_1(0) = \mathbf{d}_{10}$, $\mathbf{d}_2(0) = \mathbf{d}_{20}$. Due to the Coulomb forces acting at the discrete positions of the tracer particles we also have a fixed number of boundary conditions of the type $\mathbf{f}(s_i) = \mathbf{F}_i$ to be matched in between the end points of a fiber. Further, the tangential part of the Coulomb forces leads to a transversal stretching in the fiber. Using the relation that locally $\mathbf{v} = (0, 0, 1)$ we can easily solve the problem of forces acting in transversal direction. This means that the fiber is inextensible and unshearable an assumption that can be justified by the fact that real hair fibers show a very high tensile stiffness. Shear deformations are of rather limited interest for us so we totally neglect them.

3.2. Solving the Cosserat Equations

The above equations together with the boundary conditions form a system of coupled ODEs. Such a two-point boundary value problem (BVP) can be solved with appropriate shooting techniques. They perform recurrent integrations of the underlying ODE's while trying to minimize the distance to the boundary conditions with root finding techniques such as the Newton-Raphson method. Since the equations (10) are known to be stiff by their very nature and exhibit singularities in the solution one should at least use BVP-solvers with continuation [HM03]. Such continuation methods are superior to standard BVP-solvers but perform at slow convergence rates. Moreover, the convergence rate depends on the quality of the initial guess. In [Pai02] Pai demonstrates how to approximate the solution to the above equations by decoupling the balance laws from the kinematic relations which can be integrated explicitly by using Rodrigues' formula which is in fact equal to linearizing the rotations. This method can be used in conjunction with standard BVP-solvers to compute the Jacobian matrix. However, recurrent evaluations of this method are very expensive. Moreover, this approach operates with local forces such that each load is transformed to a follower load, a problem which we will discuss in detail later. In contrast, we pursue an approach wherein the energy functional of the rod is minimized.

3.3. Parameterizing Rotations

To solve the kinematic relation $\mathbf{d}_i' = \mathbf{u} \times \mathbf{d}_i$ it is essential to choose an appropriate parameterization for the rotations. We use exponential maps, an approach that was originally introduced to the field of rod mechanics by Simo and Vu-Quoc [SVQ88] (also used in [Pai02], [CJY02]). The exponential map maps the rotational strain vector $\mathbf{u}$ specifying the rotation axis and the magnitude of a three DOF rotation to the respective rotation. Together with the linear strain vector $\mathbf{v}$ (here always $\mathbf{v} = (0, 0, 1)$) it describes a screw motion. The relative rotation from frame $\mathcal{F}(s_i)$ to frame $\mathcal{F}(s_{i+1})$ is obtained as $e^{\hat{\mathbf{w}}\theta} \approx \mathbf{I} + \hat{\mathbf{w}} \sin\theta + \hat{\mathbf{w}}^2 \cos(1 - \cos\theta)$, and the corresponding translation as $(\mathbf{I} - e^{\hat{\mathbf{w}}\theta})\hat{\mathbf{w}}\nu + \mathbf{w}\mathbf{w}^T \nu\theta$, where $\mathbf{w} = \mathbf{u}/|\mathbf{u}|$, $\hat{\mathbf{w}} = \mathbf{w}\times$, $\nu = \mathbf{v}/|\mathbf{u}|$, and $\theta = |\mathbf{u}| \cdot d$. $d = s_{i+1} - s_i$ is the distance between two consecutive points on the curve.

3.4. Energy Minimizers

As stated before our approach is based on an energy minimization scheme which provides a solution to the Cosserat equations. Moreover, it allows us to integrate single forces acting in-between the end point of the rod. In particular, it seeks a rotational strain function $\mathbf{u}^*(s)$ that describes the minimal energy configuration of a rod subject to external forces. A similar model has been introduced by [WH04]. It is based on the differential geometry of the curves and follows the standard approach in which a space curve is equipped with a set of orthogonal directors. The orientation at each point is expressed in terms of global Euler angles. Since theses are a function of the arc length parameter they can be approximated by a linear combination of appropriate basis functions (Ritz approach). Suitable coefficients can be found

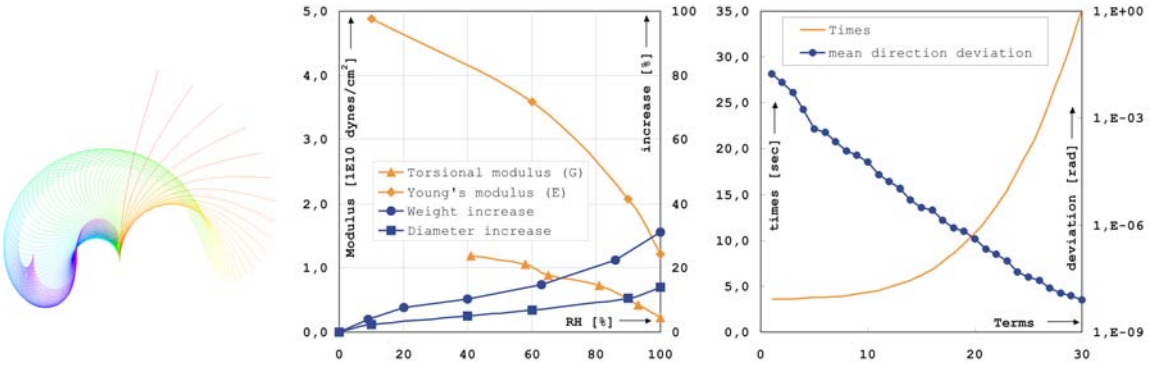

Figure 3: *Left: Sequence of deforming rods due to a terminal follower load with increasing magnitude. The direction of the terminal force remains always perpendicular to the center line of the rod. Center: Young's modulus, torsional modulus, weight and diameter of human fibers depend on the humidity (isotherms). Right: Computation times (in sec) taken with the fast multipole method for varying numbers of terms in the multipole expansion (on a Pentium IV 2.4 GHZ). The dotted line shows the corresponding mean direction deviation from the correct solution averaged over all particles.*

by solving an unconstrained optimization problem wherein the internal energy of the rod is minimized. It is normally not an easy task to find a set of basis function which are complete and can deal with the singularities caused by the use of global Euler angles. Besides, the times needed to compute the solution to simple problems (e.g., the straight rod under gravity) is comparatively large. In our approach we directly operate on the discretized data.

Our approach bases on the minimization of the internal energy of the rod which is given as the sum of the stored internal energy $\mathcal{U}^E$, the potential energy $\mathcal{U}^B$ due to body forces, and the work done by all external forces acting on the rod:

$$\mathcal{U}^T = \mathcal{U}^E - \mathcal{U}^B - \mathcal{W}. \tag{11}$$

Therefore, we assume for a hyperelastic rod the existence of an stored energy function $\Gamma = (\mathbf{v}, \mathbf{u}, s)$ such that $\mathbf{n} = \partial\Gamma/\partial\mathbf{v}$ and $\mathbf{m} = \partial\Gamma/\partial\mathbf{u}$. We then obtain the elastic energy as the integral over the entire domain Ω:

$$\mathcal{U}^E = \int_\Omega \Gamma(\mathbf{u}) \mathrm{ds}. \tag{12}$$

The stored energy is defined by the difference between the actual configuration and its reference configuration $H^C(\mathbf{u}) - H^0(\mathbf{u})$. If we choose the stored energy function to be

$$\Gamma(\mathbf{u}) = \mathrm{tr}\left\{\frac{1}{2}\mathbf{C}\cdot[\mathbf{I}(\mathbf{u}-\hat{\mathbf{u}})]^2\right\}, \tag{13}$$

the simple constitutive laws are given as the derivatives of this function. The quantities $\hat{\mathbf{u}}$ measure the rotational strains in the reference state. The stored energy function takes its global minimum in the reference configuration, thus the reference configuration is stress-free. $\mathbf{v}$ does not contribute to the energy since we have chosen the rod to be inextensible and unshearable. The C_{ii}'s are material constants where $C_{11} = EI_1$, $C_{22} = EI_2$, $C_{33} = GI_3$, and $C_{ij} = 0$ for $i \neq j$. E and G are known as Young's modulus and the torsion modulus, respectively. The quantities $I_{1,2,3}$ are the respective moments of inertia of the cross section. The directors $\mathbf{d}_1$ and $\mathbf{d}_2$ are normally chosen such that they coincide with I_1 and I_2. Since these quantities depend on the humidity as well as the temperature we have a simple model that accounts for environmental conditions. The dependencies have been determined empirically (cf. [Rob02]) and are shown in Fig. 3. Here we focus on the isotherms, i.e., the dependency on the humidity for a fixed temperature (25°C). Thus, for a given humidity we choose accordingly the stiffness parameters as well as the weight of the fiber.

Furthermore, the potential energy due to body forces like gravity is given by

$$\mathcal{U}^B = |\mathbf{g}| \int_\Omega l(s)\mathbf{r}(s)\mathbf{g}_{|\cdot|}\,\mathrm{ds}, \tag{14}$$

where l is the weight per unit length and $\mathbf{g}_{|\cdot|}$ is the unified force field vector.

3.4.1. External Forces

In principle, external forces acting at discrete points of the rod can be treated as shown in [Pai02]. The most prominent problem with this approach is that forces are considered w.r.t. to the local system of a node. A force that is dependent of the rod's configuration is called *follower load*. To illustrate the impact of follower loads let us consider a vertical rod and a terminal force that is perpendicular to the center line of the rod. Intuitively, we expect the rod to be deformed in such a way that the centerline of the rod is at most parallel to the force. If the force is given in local coordinates of

the end point then it deforms beyond the vertical shape to a semicircle because the terminal load stays perpendicular to the rod's centerline (cf. Fig. 3). As we further increase the magnitude of the force the rod assumes an *s*-like shape and so on. Each turn to the opposite side adds a hunchback to the rod. Follower loads have applications, e.g. if we want to simulate a hosepipe ejecting water. Then the reaction force is always tangential to the end of the hose. In case of the Coulomb interactions we want the forces to act w.r.t. to the global system. The work done by an external force $\mathbf{f}$ is given by $\mathcal{W} = \mathbf{f} \cdot \delta\mathbf{x}$. Thus, only displacements in the direction of the force contribute to the overall internal energy. The point of application of a force and its displacement respectively are obtained by integrating the kinematic relations, cf. Sec. 3.1. In principle, $\mathbf{f}$ can be any type of external force, Coulomb as well as contact forces or cohesion. Thus, the total work done by all external forces is

$$\mathcal{W} = \sum_i \mathbf{f}_i \cdot \delta\mathbf{r}_i. \tag{15}$$

The negative signs in eq. (11) are due to the fact that external forces add energy to the system.

As mentioned in Sec. 2 we consider the Coulomb forces due tracer particle interactions as well as those from the interaction with the scalp. Although it is possible we currently do not consider cohesive forces that stick the fibers of a single hair strand together.

3.4.2. Discretization

The total energy function to be minimized is given by eq. (11). So, we seek for a minimizer to this variational problem which describes the state where the external forces due to gravity and Coulomb force are in balance with the material internal reaction forces. Since each force induces local perturbations we discretize our domain. To solve for the equilibrium configuration we employ a conjugated gradient solver. Since the rotation vector $\mathbf{u}_i$ is given for each node the dimension of the underlying optimization problem depends on the discretization. The Jacobian matrix $\partial\mathcal{U}^T/\partial\mathbf{u}$ of the energy function can efficiently be approximated by a forward finite difference scheme. Specifically, we use an equidistant grid with a fixed size of approximately three nodes per cm. Thus, for a hair fiber of length 30 cm the underlying minimization problem has approximately 300 dimensions.

4. Results

To test our approach we drove different experiments. For this, we implemented a test environment in C++. For the multipole expansion we used the freely available DPMTA library which is written in C [Ran02]. Although this library has been implemented for parallel environments we only used the single processor mode. In order to reduce memory costs the code was fully adapted to our simulation environment such that the computations could be performed directly on our internal fiber data structure. All experiments and measurements were carried out on a Pentium IV, 2.4 GHz machine with 2 GB of RAM.

Specifically, we considered the following test cases:

1. A *curly hair tress* consisting of 300 fibers (100 segments each, length: 30 cm), uniformly distributed over an elliptic cross section.
2. As a more complex example we generated a hair style consisting of about 65,000 fibers which covered one half of a human head model (*half scalp model*).

The initial configurations were generated with our Cosserat approach. The geometric properties considered herein correspond to values found in real human hair.

Our algorithm first distributes the tracer particles over the fibers according to a given charge density and computes the Coulomb interactions. Then the new configuration of the fibers is calculated solving an unconstrained optimization problem as described in Sec. 3.4. Specifically, we used a tracer particle density of $\rho_P = 330$ particles/m. The simulation temperature was 25°C for all computations at varying relative humidity (65% and 100%). The charge density was $-7.7 \cdot 10^{-4}$ C/cm. The results can be seen in Fig. 4.

We tested two approaches for the charging: a) bringing up the full charge in a single step and b) dividing it over n steps in order to simulate the built up of the electrostatic field. For this, we assume that the amount of charge that can be absorbed by the current configuration decays logarithmically over n steps. It turns out that applying the full charge in a single step does not yield the same final configurations as when the maximum charge is applied in several subsequent steps. Applying the full charge in a single step leads to more asymmetric force distributions with larger forces on the outer fibers of the strand. In the latter case the system converges against a symmetric configuration. The cause may be that small asymmetries in the force distributions are smoothed out by the subsequent integration process of the Cosserat equations. As stated in Sec. 3.4 we solve an unconstrained optimization problem in order to find the equilibrium configurations of the fibers. This optimization process directs the global energy into a minimum and—as is known— such minima correspond to symmetric system states.

For the strand we measured the electric field strength given by $E = F/q$ and averaged it over all particles. For comparisons we consulted one of the rare publications which contains field strength measurements on human hair, an US Patent on 'static reducing' hair conditioners [Pat88]. Therein a set of pre-treated tresses were charged by combing them with 50 strokes of a rubber comb. The sensing probe of the fieldmeter was placed at a distance of 12 cm from the surface of the tresses. The values range between 20 kV/m and 120 kV/m and correspond to ours of 13 kV/m.

Furthermore, we experimented with different numbers of terms in the multipole expansion. As can be seen in Fig. 3

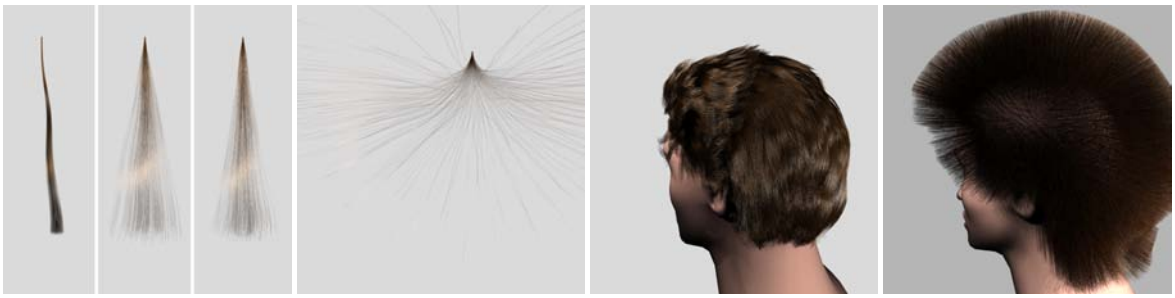

Figure 4: *The pictures show the results of our approach to electrostatics computation on human hair. 1) Curly fiber assembly consisting of* 300 *individual fibers (length* 30 *cm,* 100 *segments per fiber). 2) After applying a charge ($T = 25^{\circ}C$, RH=65%). 3) Increasing humidity to* 100%*. Note that due to the weight increase and the decrease of the stiffness parameters the fibers tend to loose their shape, an effect than can be observed in real hair. 4) Same charge but without the effect of gravity ($T = 25^{\circ}C$, RH=65%). 5) Half scalp model consisting of 65,000 fibers of equal length before and after applying a charge to both the scalp surface and the hair fibers (100 segments per fiber).*

the time increases almost quadratically with the number of terms. The blue curve shows the mean direction deviation from the exact solution obtained with the naive force computation. The angles are averaged over all particles of the strand. The deviation starts at 10^{-2} rad for two terms and decreases to a value of 10^{-9} rad. The largest mean deviation from the exact force magnitude observed was 0.3 %. Finally, we found that using more than two terms in the expansion has no effect on the visual results.

5. Conclusion and Future Work

We presented a new paradigm which is intended as a first step towards a high accuracy physical hair model covering the level of single hair fibers and the level of hair strands. This approach accurately models hair on a per fiber basis rather than employing guides with subsequent interpolation. As a first instance we have demonstrated how the effects of electrostatics on human hair can efficiently be modeled by employing multipole expansions of distributed point charges and coupling it to an equilibrium state rod model based on the special theory of COSSERAT rods. Currently, we are working on numerical simulations which capture the effects of electrostatics induced by brushing the hair. We hope that within such a simulation framework we can also tackle the question of the relation between the contributions of static electricity to the observed increase of volume of hair strands after brushing and the contributions of plastic deformation within fibers and a higher resulting curliness within the fibers of a hair strand.

References

[Ant95] ANTMAN S. S.: *Nonlinear Problems of Elasticity*, vol. 107 of *Appl. Math. Sci.* Springer-Verlag, Berlin and New York, 1995.

[BCN03] BANDO Y., CHEN B.-Y., NISHITA T.: Animating hair with loosely connected particles. In *Computer Graphics Forum (Proceedings of Eurographics 2003)* (2003), vol. 22(3).

[BH86] BARNES J., HUT P.: A hierarchical O(N log N) force-calculation algorithm. *Nature 324* (1986), 446–449.

[BKCN03] BERTAILS F., KIM T.-Y., CANI M.-P., NEUMANN U.: Adaptive wisp tree - a multiresolution control structure for simulating dynamic clustering in hair motion. In *Proceedings of the 2003 ACM SIGGRAPH/Eurographics Symposium on Computer Animation* (July 2003), pp. 207–213, 377.

[CJY02] CHANG J. T., JIN J., YU Y.: A practical model for hair mutual interactions. In *ACM SIGGRAPH Symposium on Computer Animation, San Antonio* (2002), pp. 73–80.

[CK05] CHOE B., KO H.-S.: A statistical wisp model and pseudophysical approaches for interactive hairstyle generation. *IEEE Transactions on Visualization and Computer Graphics 11(2)* (2005), 160–170.

[DYP93] DARDEN T. A., YORK D. M., PEDERSEN L. G.: The effect of long-range electrostatic interactions in simulations of macromolecular crystals: A comparison of the ewald and truncated list methods. *J. Chem. Phys. 99(10):10089* (1993).

[GR87] GREENGARD L. F., ROKHLIN V.: A fast algorithm for particle simulation. *Journal of Computational Physics 73*, 325 (1987), 325–348.

[HM03] HEALEY T. J., MEHTA P. G.: Straightforward computation of spatial equilibria of geometrically exact cosserat rods, 2003. http://tam.cornell.edu/Healey.html.

[HMT01] HADAP S., MAGNENAT-THALMANN N.: Modeling dynamic hair as a continuum. In *Computer Graphics Forum* (2001), vol. 20(3).

[Kir59] KIRCHHOFF G.: Über das Gleichgewicht und die Bewegung eines unendlich dünnen elastischen stabes. *J. F. Reine Angew. Math. 56* (1859), 285–313.

[Pai02] PAI D. K.: STRANDS: Interactive simulation of thin solids using Cosserat models. In *Computer Graphics Forum* (2002), vol. 21(3), pp. 347–352.

[Pat88] PATEL C.: Hair conditioning composition and method. United States Patent, Patent Number US04719104, 1988. http://210.69.13.146/search/PNUS04719104.

[Ran02] RANKIN W. T.: DPMTA - A distributed implementation of the parallel multipole tree algorithm - Version 3.1. Department of Electrical Engineering, Duke University, 2002. Available at `http://www.ee.duke.edu/~wrankin/Dpmta/`.

[Rob02] ROBBINS C.: *Chemical and Physical Behavior of Human Hair*, 4 ed. Springer-Verlag, New York, 2002.

[SVQ88] SIMO J. C., VU-QUOC L.: On the dynamics in space of rods undergoing large motions – a geometrically exact approach. *Computer Methods in Applied Mechanics and Engineering 66* (1988), 125–161.

[SVW05] SOBOTTKA G., VARNIK E., WEBER A.: Collision detection in densely packed fiber assemblies with application to hair modeling. In *CISST'05—The 2005 International Conference on Imaging Science, Systems, and Technology: Computer Graphics* (Las Vegas, USA, June 2005), Arabnia H. R., (Ed.), CSREA Press, pp. 244–250.

[WGL04] WARD K., GALOPPO N., LIN M. C.: Modeling hair influenced by water and styling products. In *Proceedings of the Computer Animation and Social Agents 2004* (2004).

[WH04] WAKAMATSU H., HIRAI S.: Static modeling of linear object deformation based on differential geometry. *The International Journal of Robotics Research 23*, 3 (2004), 293–311.